Nuclear quadrupole resonance and x-ray investigation of the structure of $Na_{2/3}CoO_2$

T. A. Platova,[1,2] I. R. Mukhamedshin,[1,2,*] H. Alloul,[2] A. V. Dooglav,[1,2] and G. Collin[2]
[1]*Physics Department, Kazan State University, 420008 Kazan, Russia*
[2]*Laboratoire de Physique des Solides, UMR 8502, Université Paris-Sud, 91405 Orsay, France*
(Received 6 August 2009; revised manuscript received 16 November 2009; published 18 December 2009)

We have synthesized various samples of the $x=2/3$ phase of sodium cobaltate Na_xCoO_2 and performed x-ray powder diffractions spectra to compare the diffraction with the structure proposed previously from NMR and nuclear quadrupole resonance (NQR) experiments [H. Alloul, I. R. Mukhamedshin, T. A. Platova, and A. V. Dooglav, EPL **85**, 47006 (2009)]. Rietveld analyses of the data are found in perfect agreement with those and confirm the concentration $x=2/3$ obtained in the synthesis procedure. They even give indications on the atomic displacements of Na inside the unit cell. The detailed NQR data allow us to identify the NQR transitions and electric field gradient parameters for four cobalt sites and three Na sites. The spin-lattice and spin-spin relaxation rates are found much smaller for the nonmagnetic Co^{3+} sites than for the magnetic sites on which the holes are delocalized. The atomic ordering of the Na layers is therefore at the source of this ordered distribution of cobalt charges. The method used here to resolve the Na ordering and the subsequent Co charge order can be used valuably for similar structural determinations for various phases with $x>0.45$ for which Na ordering has been established.

DOI: 10.1103/PhysRevB.80.224106 PACS number(s): 71.27.+a, 61.66.−f, 76.60.Gv

I. INTRODUCTION

Since the discovery of high thermoelectric power (TEP) (Ref. 1) and superconductivity[2] in Na cobaltates, extended efforts have been done in order to understand their magnetic and electronic properties. Anomalous magnetic properties have been discovered in unexpected ranges of Na concentrations, with an abrupt change of magnetic correlations from antiferromagnetic for $x\leq 0.62$ to ferromagnetic for $x\geq 0.67$.[3] However, a situation quite unusual in solid-state physics prevailed so far, as very few experiments have allowed to correlate these magnetic properties with Na ordering, apart for the featureless band insulator for $x=1$,[4,5] and the very peculiar $x=1/2$ phase.[6–8]

We have recently reported that a combination of nuclear magnetic resonance (NMR) and nuclear quadrupole resonance (NQR) experiments did concur to let us determine the Na order in the $x=2/3$ phase,[9] which is a nearly ferromagnetic and metallic phase which does not order magnetically down to the lowest temperatures.[10] For this particular phase, the large set of NMR data obtained in the past allowed us, when complemented by NQR data, to demonstrate finally that the ordering of the Na atoms on the Na1 and Na2 sites of the hexagonal substructure is rather simple. It results in a differentiation of the Co sites into nonmagnetic Co^{3+} sites in which the t_{2g} subshell of electronic levels is filled and a metallic kagome network of Co sites on which the doped holes are delocalized.[9]

We perform here a careful Rietveld analysis of the x-ray data which confirms the structure proposed from NMR and NQR and definitively establishes the $x=2/3$ Na content of this phase contrary to the $x=0.71$ value estimated by others from chemical analyzes of single-crystal samples.[11] Furthermore, we report in detail here the NQR data which, together with the approach developed in Ref. 9, will help in similar analyzes for other structurally more complicated cases of Na order detected for different $x>0.45$ values.

The paper is organized as follows. In Sec. II, we display the methods used to synthesize single phase samples for $x=2/3$ and display the powder x-ray spectra in which the Bragg peaks associated with the Na-ordered substructure are resolved. The best Rietveld fits allowed us to determine the slight atomic displacements of the Na atoms in the model unit cell deduced from NMR and NQR data. In Sec. III, we report the Na and Co NQR spectra and show that we could detect most of the NQR lines associated with four Co sites identified by the former combination of NQR and NMR data. Some of the low-frequency lines were however difficult to detect owing to experimental limitations. At the end of Sec. III, we show that the accurate electric field gradient (EFG) parameters can be hardly described merely by a point-charge model, even taking into account the site displacements determined by x rays. This reveals the need for more sophisticated and accurate calculations taking fully into account the atomic and electronic band structures. The spin-spin and spin-lattice relaxation data reported in Sec. IV for the four Co sites are studied and analyzed then, which allowed us to establish that both quantities can be used to distinguish the nonmagnetic cobalts from those of the more magnetic Co sites which are organized in a kagome sublattice in the $x=2/3$ phase.

II. SAMPLE PREPARATION AND LATTICE STRUCTURE

It has been established that the phase diagram of Na cobaltates is discontinuous and consists of a series of homogeneous phases extending over limited concentration ranges, separated by composition gaps.[3,10] A homogeneous domain range is characterized by a specific Na ordering which one can monitor by powder x-ray diffraction experiments.

A. Sample synthesis

We have evidenced that in pure oxygen atmosphere the compound with $x=2/3$ is stable in the temperature range of

600–700 °C. Phases with higher Na content are stabilized at higher temperatures, which for a nominal composition $x=2/3$ releases some Co_3O_4. Conversely, lower preparation temperatures favor phases with $x<2/3$ and in such case, the excess Na is somewhat difficult to detect by diffraction, although after treatment in air, the characteristic diffractions of Na_2CO_3 appear. So to retain the $x=2/3$ phase in powders, the samples were directly introduced in a furnace stabilized at 700 °C and were then quenched in a few seconds from the synthesis temperature to room temperature by pouring the powder on a copper plate. Three different approaches have been used to synthesize single-phase materials:

(1) Direct synthesis from a stoichiometric composition of Co_3O_4 and Na_2CO_3. However, we found that the reaction is rather slow at such low temperatures and requires weeks of treatment with intermediate grindings to eliminate the last traces of unreacted Co_3O_4.

(2) From a mixture of cobaltates with calibrated compositions synthesized previously [such as $Na_{1/2}CoO_2$ and $Na_{0.71}CoO_2$ (Ref. 10)] taken in a proper ratio.

(3) By deintercalation of Na from $Na_{0.71}CoO_2$ by annealing it at 700 °C—out of its own stability temperature range. In that case, the composition $x=2/3$ of the dominant phase stabilized differed from the initial nominal composition $x=0.71$ of the material. The average Na content of the material which would be detected by chemical analysis remained unchanged at $x=0.71$. The released Na remained in excess and not well crystallized (or oxidized) and was difficult to observe directly by x rays. We could evidence its presence by annealing again the material at $T>800$ °C in oxygen. This restored the initial $x=0.71$ material with its characteristic diffraction pattern and lattice constants.

Overall, the second method was found the most reliable and was easily reproducible.

B. Rietveld refinement of the structure

As already indicated in a previous published report,[9] the NMR and NQR data have allowed us to identify three Na and four Co sites, their occupancies, and those with axial symmetry in the lattice. It has been then possible to establish the two-dimensional (2D) Na ordering on the Na1 and Na2 sites of the usual hexagonal structure, the differentiation of Co sites shown in Fig. 1, as well as the three-dimensional (3D) stacking. Such a structure ought to be recovered by x-ray scattering experiments.

Data collection for the diffraction patterns was performed on a conventional Philips powder diffractometer using Cu $K\alpha$ radiation, 2θ range 10°–130°, step of 0.03°, and counting time 18 s per point. As shown in Fig. 2, diffraction patterns systematically revealed the occurrence of an appreciable number of weak satellites, however with significant intensities, in addition to the usual strong substructure reflections. This is a constant feature of sodium cobaltate materials. Indeed, for the phases with $x>0.5$, we have detected such sets of satellites, which in most cases can be described by a single incommensurate wave vector with component q_b^*. Under these conditions, the lattice loses the hexagonal symmetry and becomes generally orthorhombic with

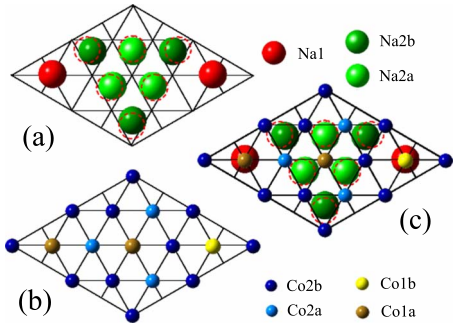

FIG. 1. (Color online) $Na_{2/3}CoO_2$ structure model. Two neighboring sodium and cobalt layers are shown in one unit cell size. The (a) upper plane illustrates the Na ordering and the (b) lower one the differentiation in the Co plane. Dotted circles represent the displaced positions of the sodium ions, as deduced from the x-ray data analysis. The diameters of the Na and Co ions scale with the atomic radii of the corresponding ions. (c) Top view of the two considered Co and Na planes.

$a_{ort}=a_{hex}\sqrt{3}$, $b_{ort}=a_{hex}/q_b^*$, and $c_{ort}=c_{hex}$, as was noticed early by Zandbergen *et al.* from high-resolution microscopy experiments.[6] This has led to propose a phenomenological model[3] in which an increase of Na content corresponded to the insertion of "stripes" of Na2 with increasing a_{ort} in the known structure of $Na_{1/2}CoO_2$. It is easy to evaluate that in such a model, the empirical relation $x=1-q_b^*$ applies. In contrast, our particular composition exhibits a commensurable locking leading to a conventional superstructure.

The crystal structure was simply deduced from previous results:

(1) NMR-NQR data indicated the separation of cationic sites into seven distinct positions, four for cobalt and three for sodium, and gave indications concerning their cationic surrounding.

(2) From chemistry results, pure phases were obtained by mixtures of calibrated starting materials only for ionic concentration strictly limited to sodium content x close to 2/3 per unit formula. This was confirmed by the position of the c lattice-constant value on the curve $c=f(x)$ which confirmed this value of 2/3 for sodium concentration.

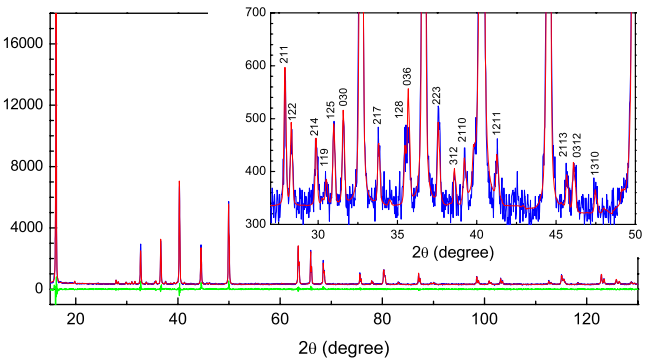

FIG. 2. (Color online) $Na_{2/3}CoO_2$ structure determination. (Main field) X-ray diffraction pattern observed I_{obs} in blue, calculated I_{calc} in red, and $I_{obs}-I_{calc}$ in green. The intense 002 substructure reflection at $2\theta\approx16°$ is not used for the refinement calculation because of its strong instrumental asymmetry. (Insert) Intensities of satellite reflections: blue observed, red calculated.

TABLE I. X-ray determination of the structure of $Na_{2/3}CoO_2$, data collection $2\theta=10-130°$, Cu K_α. $a=9.8007(1)$ Å; $3c=32.8151(4)$ Å; space group $R\text{-}3c$ ($n°167$), hexagonal axes, $Z=72$, $R=5.41\%$, and $R_w=7.16\%$.

Site	Position[a]	x	y	z	B
Co1b	6 b	0	0	0	0.34(2)
Co1a	12 c	0	0	0.3315(3)	
Co2a	18 d	1/2	0	0	
Co2b	36 f	1/3(0.0005)	1/6(0.0006)	0(0.0003)	
Na1	12 c	0	0	1/12	0.52(7)
Na2a	18 e	0.632(2)	0	1/4	
Na2b	18 e	0.187(2)	0	1/4	
Ox-1	36 f	1/6[b]	0[b]	0.0298(5)	1.3(2)
Ox-2	36 f	2/3[b]	0[b]	0.0290(4)	
Ox-3	36 f	1/2[b]	1/6[b]	0.0320(5)	
Ox-4	36 f	1/6[b]	1/2[b]	0.0295(5)	

[a]Number of sites and Wyckoff notation for position. All sites are found to be fully occupied (see text).

[b]All deviations with respect to positions given in the table are lower than calculated standard deviations, 0.002 for all x and y coordinates (see text).

(3) A decisive contribution was given by *ab initio* calculations of Hinuma *et al.*[12] leading, for the particular $x=2/3$ composition, to a planar ordering of sodium and cobalt in a $2a\sqrt{3}*2a\sqrt{3}$ which were perfectly consistent with the NMR/NQR data (a=hexagonal substructure lattice constant).

(4) From our phenomenological model, we had first proposed a $a\sqrt{3}*3a*3c$ (i.e., $q_b^*=1/3$) superstructure cell. Most superstructure reflections could be indexed within this hypothetical cell, with the exception of a few weak ones. However, the calculated intensities could not fit the observed diffraction pattern. In fact, the true superstructure cell calculated in Ref. 12 corresponds to a cell twice larger. The essential point was then that the 3D packing proposed from the NMR and NQR data[10] corresponds unambiguously to a $3c$ lattice constant as well.

Consequently, the packing of the Hinuma *et al.*[12] planar organization in a 3D lattice leads straightforwardly to a rhombohedral superstructure unit cell $2a\sqrt{3}*2a\sqrt{3}*3c$, space group $R\text{-}3c$ ($n°167$) (see Table I), which was immediately found to describe all the details of the weak satellites detected, as can be seen in Fig. 2. Starting from that, the refinement strategy was purely conventional:

(i) The superstructure positions are directly deduced from the substructure which leads to four cobalt and oxygen sites all of them being fully occupied. In the same way, only three distinct well-defined sodium positions Na1 and Na2 (a and b) are concerned by that ordering.

(ii) We have first verified that these three sites are fully occupied. Indeed, we found for the occupancy of the three sites: Na1, 1.02(3); Na2a, 1.02(2), and Na2b, 0.98(2).

(iii) We have further taken one by one all the other sodium sites deduced from the substructure description and expected to be unoccupied: none of them exhibited any significant occupation within the limit of standard deviations: occupancy for Na1 sites: 0.02(2), 0.04(4), 0.03(2), respectively, for the $6a$, $18c$ ($x=1/2$), and $36f$ ($x=1/3, y=1/6, z=1/4$) positions and 0.03(2) for the $36f$ ($x=1/2, y=1/6, z=1/4$) Na2 position.

Most of the ionic coordinates are unchanged with respect to the substructure positions (footnote in Table I) at the noticeable exception of both Na2 positions. The displacements of Na2 sites already were mentioned in the Refs. 13 and 14 but it was attributed to the repulsion of randomly located neighboring Na ions, locally violating the hexagonal symmetry. But as one can see in Fig. 1, the relaxation of position of these sites corresponds to a dilatation of the Na2 triangles, which agrees with the interionic repulsion in this highly charged region. As might be expected, the displacements of Na along the honeycomb lattice (ionic conduction channel) of the outer Na2b triangle are nearly twice larger than those of the inner Na2a triangle.

Finally, we would like to mention that we have analyzed the diffraction spectra for eight distinct samples and found in all cases that the Co1a position is slightly shifted along the c-axis direction toward the Na2 trimers, with the same offset $\approx 0.06(1)$ Å. The oxygen ions are only found slightly displaced with respect to the ideal unit cell, which points the compactness of the CoO_2 slabs between which are inserted the Na ions. To conclude, the result of this Rietveld analysis definitively confirms the $x=2/3$ composition which may be expressed as $Na1_{1/6}Na2_{1/2}CoO_2$, detailed formula in perfect agreement with previously mentioned magnetic-resonance results.

III. NQR SPECTRA AND EFG PARAMETERS

A nucleus with nuclear spin $I>1/2$ has an electric-quadrupole moment in addition to its nuclear magnetic moment. The nucleus interacts with the electronic environment not only through magnetic hyperfine couplings due to its magnetic moment, but also through the interaction of its quadrupole moment with the local crystal EFG, either static or dynamic. The EFG arises from a nonsymmetric distribution of electric charge around the nucleus. This charge can originate from nonbonding electrons, electrons in the bonds, and charges of neighboring atoms or ions. Therefore, NQR is a sensitive tool for studying solids as it provides detailed information on the static and the dynamic properties of the structure on the scale of a few interatomic spacings. Thus, NQR may be regarded as a powerful tool for investigating the local order in solids whereas the interpretation of the data on disordered (or complex-ordered) materials from usual scattering experiments, such as x-ray or neutron scattering, is complicated by the absence of the long-range order translational symmetry or large and complicated unit cell.

Therefore, to demonstrate these advantages of NQR to the non-NMR specialist, we start this section by a brief NQR background introduction (Sec. III A) and describe in (Sec. III B) the basic features of the experimental techniques used. Next we show the ^{23}Na NQR spectrum (Sec. III C) and compare it to the ^{23}Na NMR data.[15] We present then (Sec. III D) the ^{59}Co NQR spectrum and show how fast- and slow-relaxing cobalt sites can be separated in the spectrum. Fi-

nally, in (Sec. III E), we show that the accurate EFG parameters can hardly be described merely by a point-charge model, even taking into account the site displacements determined by x rays.

A. NQR Background

If the crystal-field symmetry is lower than cubic, the Hamiltonian of the quadrupolar interaction can be written as[16]

$$\mathcal{H}_Q = \frac{h\nu_Q}{6}[3I_Z^2 - I(I-1) + \eta(I_X^2 - I_Y^2)], \quad (1)$$

where the quadrupole frequency

$$\nu_Q = \frac{3eQV_{ZZ}}{2I(2I-1)h}$$

is defined by the nuclear quadrupole moment Q and the largest principal-axis component V_{ZZ} of the EFG tensor and $\eta=(V_{XX}-V_{YY})/V_{ZZ}$ is the asymmetry parameter (here, the principal axes of EFG tensor are selected such as $|V_{ZZ}|\geq|V_{YY}|\geq|V_{XX}|$). In NQR experiments, the magnetic transitions between energy levels with $\Delta m=\pm 1$ are observed.

B. Experimental techniques

The NQR measurements were done using a home-built coherent pulsed NMR/NQR spectrometer. NQR spectra were taken "point by point" with a $\pi/2-\tau-\pi$ rf pulse sequence by varying the spectrometer frequency in equal frequency steps in the range of 1.5–15 MHz at 4.2 K. The detailed NQR spectra were then constructed using a Fourier mapping algorithm.[17,18]

For the low frequencies used in these experiments, the change of the tuning frequency of the sample coil immersed in the cryostat has been done with a capacitor located at room temperature outside the cryostat. In such a process, the Q factor of the probe (and the sensitivity of the spectrometer) varies considerably with frequency. This limits seriously the accuracy of absolute intensity measurements of NQR signals. Relative intensity measurements could only be done accurately for lines occurring in a narrow frequency range.

Due to the spin-spin relaxation process (which will be discussed in detail later), the intensity of the observed spin-echo NQR signal decreases with increasing delay τ between the RF pulses. It is usually impossible to reduce this time to zero, as the receiver is overloaded by the RF pulse and only recovers after a minimum time τ_R. Furthermore, for short values of τ, the detected signal is heavily distorted by residual oscillations (called "ringing") of the probe components and contains artifacts. To reduce the probe-ringing time, a low Q factor NQR probe has been used with $Q\approx 10-20$. So, the signal can only be detected after a minimum time τ_D ("dead time") which usually increases markedly with decreasing frequency. In our experiments, the minimum practical τ values varied from 70 μs at 1.5 MHz to 40 μs at 9 MHz.

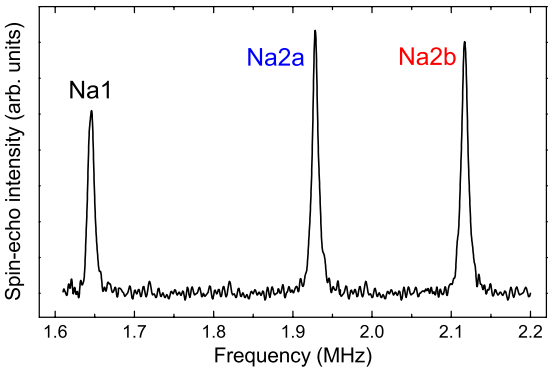

FIG. 3. (Color online) ^{23}Na NQR spectrum in the $Na_{2/3}CoO_2$ compound measured at 4.2 K. The fully resolved quadrupole structure for the three Na sites is discussed in the text.

C. ^{23}Na NQR spectrum

The nuclear-spin energy levels splitted by the EFG are doubly degenerate [see Eq. (1)]. So for ^{23}Na for which $I=3/2$ a single resonance line which corresponds to the $\pm\frac{1}{2}\leftrightarrow\pm\frac{3}{2}$ transition can be observed at the frequency

$$\nu = \nu_Q\sqrt{1+\frac{1}{3}\eta^2}. \quad (2)$$

The NQR spectrum of ^{23}Na in the $Na_{2/3}CoO_2$ compound measured at 4.2 K is shown in Fig. 3. It consists of three well-resolved narrow lines which correspond to three Na sites with distinct local environment. Such a spectrum with resolved narrow lines undoubtedly confirms that this phase is well ordered, as was pointed out in the earlier NMR study which has established that a characteristic signature of the $x=2/3$ phase[15] is to exhibit three distinct sodium sites. The shape of the ^{23}Na NQR lines has been fitted by a Lorentzian function and their positions and linewidths (which were taken as a full width at half maximum—FWHM) are collected in Table II.

As for $I=3/2$, the NQR frequency determined by Eq. (2) depends on both ν_Q and η. It is impossible to determine both parameters from the NQR spectrum. However, these parameters were determined by NMR for each sodium site and are also listed in Table II. Using these values and following Eq. (2), one can calculate the expected frequencies f_{calc} of ^{23}Na NQR lines (Table II). As one can see the calculated and

TABLE II. Comparison of ^{23}Na NQR and NMR results. ν_{calc} is the calculated value for the NQR resonance line frequency using Eq. (2) for the values of ν_Q an η obtained by NMR (see text).

	NQR		NMR[a]		
Site	ν (MHz)	$\Delta\nu$ (kHz)	ν_Q (MHz)	η	ν_{calc} (MHz)
Na1	1.645(1)	8.2(1)	1.645(5)	0.01(1)	1.645
Na2a	1.928(2)	8.2(1)	1.74(1)	0.84(2)	1.93
Na2b	2.117(1)	9.0(1)	1.86(1)	0.89(2)	2.09

[a]Reference 15.

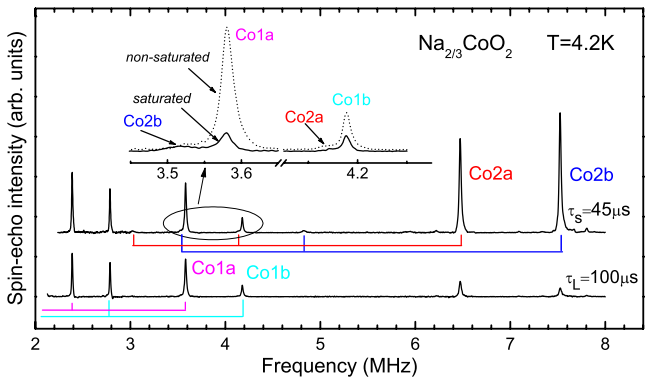

FIG. 4. (Color online) Main panel: ^{59}Co NQR spectra taken at 4.2 K for short (τ_S=45 μs) and long (τ_L=100 μs) delay between pulses. Insert: the two weak-intensity lines of the $\pm 3/2 \leftrightarrow \pm 5/2$ Co2a and Co2b sites are revealed by saturation of the high-intensity slow-relaxing lines.

experimental values are in perfect agreement, therefore the notation proposed in Ref. 15 for different sodium sites has been used in Table II. The tiny (<1.3%) difference in the experimental and calculated frequencies for the Na2b site can be easily explained by a small deviation (not more than 5°) of the Z principal axis of the EFG tensor and the c crystallographic axis for this site. The relative intensities of sodium lines will be discussed later in Sec. IV of this paper.

D. ^{59}Co NQR spectrum

Former ^{59}Co NMR data[19] taken on this phase have already allowed us to evidence distinct Co NMR lines, but the NMR spectra were somewhat difficult to analyze fully, as one needs to determine altogether the EFG parameters and NMR shifts of the various sites. The experiments were furthermore complicated by the need of a quasiperfect alignment of the powder sample with respect to the applied magnetic field. They however allowed us to determine some of the EFG parameters, which allowed us to know beforehand the range of expected ν_Q values. After a presentation of the spectra, we explain in some details how the various transitions pertaining to the same sites can be identified. The identification of the Co NQR lines is explained in some details and allows us then to determine the EFG values.

1. Experimental results

Typical NQR spectra of ^{59}Co in the $Na_{2/3}CoO_2$ compound are shown in Fig. 4. We found that the number of lines and their intensities in the observed spectrum depend strongly on the delay τ between pulses. This corresponds to the fact that the experimental spin-echo intensity depends on the rate of the spin-spin relaxation process. Consequently, the fast relaxing nuclei are not observable at long-enough delay τ between pulses, as will be detailed in Sec. IV. In the spectrum observed with the shortest possible τ_S=45 μs, there are six narrow intense lines and several lines with weaker intensity (Fig. 4). At the same time in the spectrum measured with τ_L=100 μs, the intensities of the high-frequency lines greatly decrease, while the intensities of four low-frequency

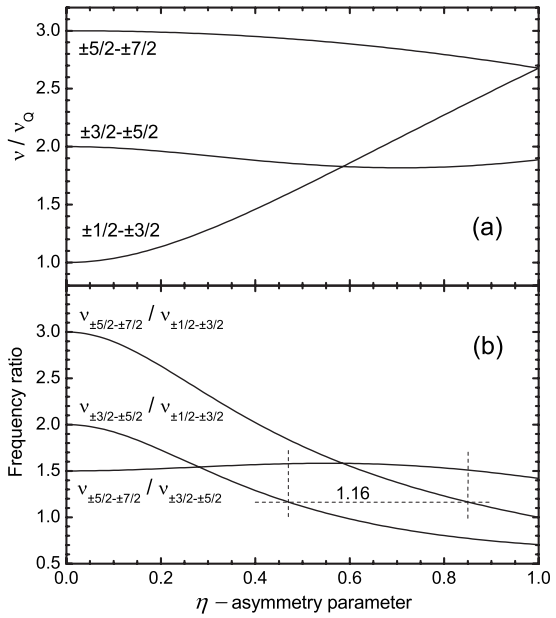

FIG. 5. (a) Theoretical dependence of the allowed NQR transition frequencies on the asymmetry parameter η of the EFG tensor for a nuclear spin I=7/2. (b) Frequency ratios of the allowed transitions plotted vs η. The particular case of the ratio 1.16 used in the text to illustrate the analysis is shown by dotted lines.

narrow lines does not change a lot. So, it is obvious that in this phase with x=2/3, two different types of Co sites—fast and slow relaxing—coexist, as was established already by NMR.[19]

As was shown earlier[3,10] for the high sodium content range (x>0.5) of the sodium cobaltates phase diagram, a cobalt charge disproportionation into Co^{3+} and $Co^{\approx 3.5+}$ is a quite common picture. Cobalt ions in sodium cobaltates are in low spin configurations, so Co^{3+} has an electronic spin S=0 and relax rather slowly in comparison to the cobalts with higher charge state on which holes delocalize (formally Co^{4+} should have S=1/2).

2. Identification of the NQR lines

As the ^{59}Co nuclei have I=7/2, for a single crystallographic site, one should observe up to three lines in the NQR spectrum. The positions of these lines depend on both ν_Q and η. Figure 5(a) shows the theoretical dependence of NQR frequencies of the allowed transitions on the asymmetry parameter of the EFG tensor for nuclear spin 7/2. These data were obtained by numerical diagonalization of the main Hamiltonian recalled in Eq. (1). One can see that the frequencies of the $\pm\frac{3}{2} \leftrightarrow \pm\frac{5}{2}$ and $\pm\frac{5}{2} \leftrightarrow \pm\frac{7}{2}$ transitions weakly depend on the asymmetry parameter η, contrary to that of the $\pm\frac{1}{2} \leftrightarrow \pm\frac{3}{2}$ transition [Fig. 5(a)]. For η=1, only two resonance lines in the spectrum should be observed. Measuring experimentally the resonance frequencies for different transitions should allow then to determine both ν_Q and η for I=7/2.

Since the number of lines in the experimental ^{59}Co NQR spectrum (Fig. 4) is much larger than 3 (number of the observable NQR lines for I=7/2), an analysis has to be done to

determine the triplet of lines which are associated with a given cobalt site in the unit cell of this $x=2/3$ compound. The basic data which can be used for such an analysis are the theoretical ratios of frequencies of different transitions for a single cobalt site which are restricted as established from Fig. 5(b).

Let us consider as an example the two intense lines at ≈7.52 and ≈6.47 MHz (Fig. 4) which corresponds to an experimental frequency ratio ≈1.16. Although we know from NMR experiments[19] that those EFG values correspond to distinct Co sites, we want to show here that a simple analysis of the NQR spectra does confirm that point. In theory, such a ratio could be found for a single site with EFGs with $\eta=0.47$ or $\eta=0.85$ [see Fig. 4(b)]. As $\eta=0.47$ corresponds to the ratio of frequencies of $\pm\frac{3}{2}\leftrightarrow\pm\frac{5}{2}$ and $\pm\frac{1}{2}\leftrightarrow\pm\frac{3}{2}$ transitions, then one should find in the spectrum a line corresponding to the $\pm\frac{5}{2}\leftrightarrow\pm\frac{7}{2}$ transition at a frequency $\approx 7.52*1.578\approx 11.87$ MHz. We indeed did not find such a line in our experiment. Also, we know from NMR that such large EFG values do not exist.[19] Similarly for $\eta=0.85$, one should find a line for the $\pm\frac{3}{2}\leftrightarrow\pm\frac{5}{2}$ transition at $7.52/1.51\approx 4.98$ MHz which does not exist either. Therefore, the ≈7.52 MHz and ≈6.47 MHz lines cannot be attributed to the same cobalt site and correspond to two different fast relaxing cobalt sites Co2b and Co2a.

Then one has to consider the next pair of lines, e.g., at ≈7.52 and ≈4.83 MHz. The frequency ratio is equal to ≈1.56 and three possible values of η should be considered. However, only one value of $\eta\approx 0.36$ gives the right third line position in the spectrum, a weak and broad line at ≈3.52 MHz which completes the spectrum of the Co2a site. We found this line by observing the slight asymmetry of the shape of the intense and narrow slow-relaxing line at 3.581 MHz, which decreases with increasing τ. To better resolve this line, we used the fact that slow- and fast-relaxing cobalts can be separated also by the large difference in their spin-lattice relaxation rates, as seen by NMR and as detailed later in Sec. IV. To saturate the signal, an additional $\pi/2$ pulse with 100 μs delay was used before the $\pi/2-\tau-\pi$ pulse sequence. In the spectrum obtained after such a pulse sequence ("saturated" in the insert of Fig. 4), the intensities of the slow-relaxing cobalt lines decrease and the lines of the fast-relaxing cobalts can be better resolved. This method allowed us to detect one more fast-relaxing line at 4.145 MHz which completes the three-line spectrum for the second fast-relaxing Co2a site, with the two other lines at 6.473 and 3.03 MHz.

Such an analysis allowed us also to determine that the two slow-relaxing lines at 3.581 and 4.178 MHz are the $\pm\frac{5}{2}\leftrightarrow\pm\frac{7}{2}$ transitions of two different sites of cobalt, Co1a and Co1b, as could already be anticipated from the Co NMR data.[19] The corresponding $\pm\frac{3}{2}\leftrightarrow\pm\frac{5}{2}$ transitions are at 2.387 and 2.785 MHz. We did not attempt to observe the $\pm\frac{1}{2}\leftrightarrow\pm\frac{3}{2}$ transitions for these slow-relaxing cobalts which should appear at low frequencies ≈1.19 and ≈1.39 MHz, outside of the frequency range of our spectrometer.

3. ^{59}Co EFG parameters

All the observed ^{59}Co NQR lines were fitted by Lorentzian functions and their positions and linewidths are collected in Tables III and VI, respectively. The values of ν_Q and η found in this work are in perfect agreement with those quoted in the Ref. 19. The fact that we observe a limited number of narrow and well-resolved ^{59}Co NQR lines (Fig. 4) confirms the existence of long-range order in this $x=2/3$ phase of sodium cobaltates. Moreover, NQR is clearly able to distinguish the charge segregation between the slow-relaxing nonmagnetic Co^{3+} (sites Co1a and Co1b) and the fast-relaxing cobalt sites Co2a and Co2b, on which holes are delocalized. Despite all our efforts, we have not found in the ^{59}Co NQR spectrum any traces of the Co3 site anticipated from NMR (see Ref. 19). As explained in the Ref. 9, we did conclude that this apparent "site" was an experimental artifact due to imperfect alignment of the NMR sample. This point will be detailed in an extensive experimental report of the Co NMR spectra.[20] The intensities of the ^{59}Co NQR lines will be discussed later in Sec. IV after the analysis of the spin-spin relaxation of these cobalt NQR signals.

TABLE III. Measured frequencies for the NQR transitions of the four Co sites in $Na_{2/3}CoO_2$ and deduced values of ν_Q and η.

	Frequency (MHz)				
Site	$\pm\frac{1}{2}\leftrightarrow\pm\frac{3}{2}$	$\pm\frac{3}{2}\leftrightarrow\pm\frac{5}{2}$	$\pm\frac{5}{2}\leftrightarrow\pm\frac{7}{2}$	ν_Q (MHz)	η
Co1a		2.387(1)	3.581(2)	1.193(1)	≤0.017
Co1b		2.785(1)	4.178(1)	1.392(1)	≤0.016
Co2a	3.03(1)	4.145(3)	6.473(1)	2.187(1)	0.362(5)
Co2b	3.52(1)	4.826(2)	7.524(1)	2.541(1)	0.358(4)

4. NQR linewidths

The broadening of the Co1 and Co2 groups of lines were found to display different behaviors likely linked with their different magnetic properties. Figure 6 shows the linewidths variation with resonance frequency of the various transitions for each of the cobalt NQR lines. Two different behaviors appear clearly: the linewidths increase with increasing frequency for Co1 sites while the opposite holds for the Co2

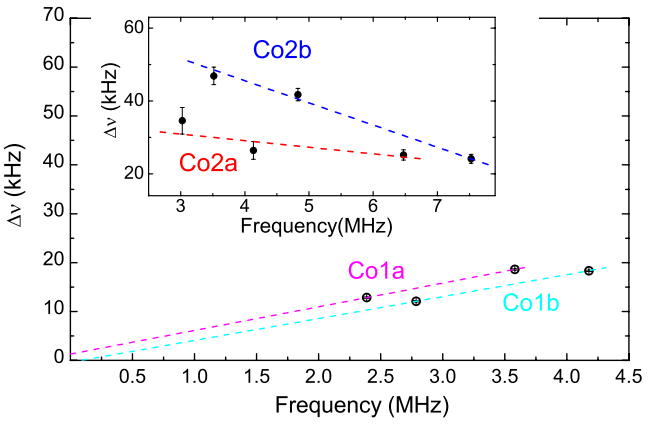

FIG. 6. (Color online) Line widths at half height for the NQR transitions of the different sites. The main panel is for Co1a and Co1b and inset for Co2a and Co2b sites.

sites. The Co1a and Co1b sites are nonmagnetic with localized holes and one expects essentially a broadening due to a distribution of EFG values. Indeed for a spin 7/2 system with zero asymmetry parameter (Co1 case), a spread $e\Delta q$ of EFG values induces broadenings of the different NQR transitions such that $\Delta\nu_i/\nu_i \propto \Delta q/q$, so that the linewidth increases linearly with the frequency of the transition as found in the data of Fig. 6. One would expect then a linewidth of ≈6 kHz for the lowest $(\pm\frac{1}{2} \leftrightarrow \pm\frac{3}{2})$ transitions of the Co1a and Co1b sites. Extrapolating the linear fits for Co1a and Co1b sites to zero frequency gives a very small residual value ≈1 kHz, which could be attributed to dipole-dipole coupling as will be detailed in Sec. IV.

As Co2a and Co2b are magnetic sites, a broadening due to magnetic interactions might take place and apparently increases with decreasing index of the quadrupole transition. This will be discussed in Sec. IV after considering the spin-spin T_2 processes.

E. Rough estimates of the EFG values

We have calculated the EFG tensors and the corresponding parameters of the quadrupole Hamiltonian (ν_Q and η) for all sites of the ^{23}Na and ^{59}Co in the simplest point-charge model assuming charges 1^+ on Na, 3^+ on Co1, 3.44^+ on Co2, and 2^- on O (see Table IV). Of course, one does not expect such point-charge calculations to fit perfectly the data as similar calculations do not even explain the simple case of Na_1CoO_2 for which all Co are Co^{3+} (Ref. 4 and references therein). Such an approach does not take into account correctly the cobalt-oxygen covalency. We do however clearly see in the results displayed in the Table IV that for the Na1 and Co1 sites, the asymmetry parameter is of course that expected from the site symmetry, that is $\eta=0$. We also find that the asymmetry of the structure yields rather large asymmetries for the EFG values on the Na2 and Co2 sites as found experimentally. However, the magnitudes of the EFG computed do not agree quantitatively with the experimental values. We did however find that the displacement of the Na atoms found in the x-ray structure analysis yields significant changes in the calculated EFG values. This reveals that more sophisticated calculations taking into account the atomic displacements and the band structure at least in the local-density approximation (LDA) are required to explain the EFG parameters.

TABLE IV. Results of the point-charge model calculations of the EFG parameters for established structure of the $Na_{2/3}CoO_2$. All quadrupolar frequencies ν_Q are in MHz. θ (in degree) is the angle between the Z principal axis of the EFG tensor and the c crystallographic axis. Na: quadrupole moment $^{23}Q=0.1$; Sternheimer antishielding factor $^{23}\gamma=-4.1$; Co: $^{59}Q=0.42$; $^{59}\gamma=-7$.

Site	Experiment	Nonshifted	shifted
Na1	$\nu_Q=1.645(5)$	$\nu_Q=0.61$	$\nu_Q=0.28$
	$\eta=0$	$\eta=0$	$\eta=0$
	$\theta=0$	$\theta=0$	$\theta=0$
Na2a	$\nu_Q=1.74(1)$	$\nu_Q=0.93$	$\nu_Q=0.94$
	$\eta=0.84(2)$	$\eta=0.88$	$\eta=0.19$
	$\theta=0$	$\theta=90$	$\theta=90$
Na2b	$\nu_Q=1.86(1)$	$\nu_Q=0.53$	$\nu_Q=1.15$
	$\eta=0.89(2)$	$\eta=0.31$	$\eta=0.36$
	$\theta\leq 5$	$\theta=90$	$\theta=90$
Co1a	$\nu_Q=1.193(1)$	$\nu_Q=1.06$	$\nu_Q=1.71$
	$\eta\leq 0.017$	$\eta=0$	$\eta=0$
		$\theta=0$	$\theta=0$
Co1b	$\nu_Q=1.392(1)$	$\nu_Q=1.18$	$\nu_Q=0.94$
	$\eta\leq 0.01b$	$\eta=0$	$\eta=0$
		$\theta=0$	$\theta=0$
Co2a	$\nu_Q=2.187(1)$	$\nu_Q=1.42$	$\nu_Q=1.55$
	$\eta=0.362(5)$	$\eta=0.26$	$\eta=0.56$
		$\theta=18$	$\theta=14$
Co2b	$\nu_Q=2.541(1)$	$\nu_Q=1.55$	$\nu_Q=1.37$
	$\eta=0.358(4)$	$\eta=0.56$	$\eta=0.40$
		$\theta=11$	$\theta=12$

IV. SPIN-LATTICE RELAXATION AND SPIN-SPIN RELAXATION

When thermal equilibrium of the nuclear spins is disturbed by RF pulses, their equilibrium magnetization is recovered by the nuclear spin-lattice relaxation (NSLR) process which corresponds to the relaxation of the longitudinal component of the magnetization. The decay of the transverse component of the magnetization, the nuclear spin-spin relaxation (NSSR) process, is connected with the loss of coherence inside the spin system due to spin-spin interactions. Generally, both relaxation processes could have different origins which reflect magnetic and electronic properties of the materials, the inner arrangement, the interactions in the spin system, and the different motion and diffusion processes. In this section, we report and discuss first in Sec. IV A the ^{59}Co spin-lattice relaxation for all four cobalt sites. Next we consider in Sec. IV B the spin-spin relaxation starting from ^{23}Na as a simple case of NSSR. Then we analyze the ^{59}Co spin-spin relaxation. We demonstrate that both NSLR and NSSR allow to differentiate the two types of Co sites—nonmagnetic Co^{3+} ions on 25% of the cobalt sites and a metallic Kagome network of Co sites on which the doped holes are delocalized.[9]

A. ^{59}Co spin-lattice relaxation

To study the NSLR process, we have used the magnetization inversion recovery method which uses three pulses: $\pi - t - \pi/2 - \tau - \pi$, where t and τ are the time intervals between pulses. In this sequence, the first pulse rotates the magnetization by 180°, the second and third pulses give a spin echo, and the dependence of the spin-echo intensity on delay time t allows to monitor the recovery of the nuclear magnetization associated with a given NQR transition

$$M(t) = M_0[1 - BR(t)]. \quad (3)$$

Here, M_0 is the thermal equilibrium value of magnetization and the parameter B characterizes the actual magnetiza-

TABLE V. Theoretical spin-lattice relaxation function (4) parameters for different ^{59}Co sites for the case of magnetic relaxation by weak isotropic fluctuating magnetic fields (based on Ref. 22).

Site	η	Transition	a_1	λ_1	a_2	λ_2	a_3	λ_3
Co1	0	$\pm\frac{5}{2}\leftrightarrow\pm\frac{7}{2}$	0.14	21	0.65	10	0.21	3
		$\pm\frac{3}{2}\leftrightarrow\pm\frac{5}{2}$	0.74	21	0.16	10	0.1	3
Co2	0.36	$\pm\frac{5}{2}\leftrightarrow\pm\frac{7}{2}$	0.27	17.7	0.53	8.96	0.2	3
		$\pm\frac{3}{2}\leftrightarrow\pm\frac{5}{2}$	0.88	17.7	0.038	8.96	0.082	3

tion after the first pulse at $t=0$ (the imperfection of the experimental conditions gave typical values $B\simeq 1.8$ rather than $B=2$ expected for a perfect π pulse). The shape of the relaxation function $R(t)$ depends on the nuclear transition sampled. For a two-level nuclear system (such as the $I=3/2$ NQR case), this process is exponential $R(t)=\exp(-t/T_1)$, with a characteristic time constant T_1, the spin-lattice relaxation time.[21] But generally for $I>1/2$, the nuclear energy levels are differentiated by the quadrupole interaction with the crystalline electric field [Eq. (1)]. As a consequence, the difference in population between adjacent levels which are probed by the RF pulses depends on the populations of the levels which are not hit by the RF pulses. Therefore, the magnetization recovery becomes multiexponential

$$R(t)=\sum_i a_i \exp\left(-\frac{\lambda_i t}{T_1}\right), \tag{4}$$

but is still characterized by a single T_1 value.

The spin-lattice relaxation could be driven either by magnetic or quadrupolar fluctuations. However, in the sodium cobaltates, which exhibit unusual magnetic properties, the magnetic relaxation mechanism dominates at least at low T. Following Ref. 22, we obtained the parameters for the theoretical relaxation functions $R(t)$ for the case of magnetic relaxation by weak isotropic fluctuating magnetic fields for different transitions of different Co sites (see Table V).

Figure 7 shows experimental spin-lattice relaxation curves for the $\pm\frac{5}{2}\leftrightarrow\pm\frac{7}{2}$ and $\pm\frac{3}{2}\leftrightarrow\pm\frac{5}{2}$ transitions for the Co2b site measured at 7.52 and 4.83 MHz, respectively. The fits with Eq. (4) with the a_i and λ_i taken from Table V are shown by solid lines. These fits give T_1 values of 0.73(4) and 0.8(1) ms, respectively, for the $\pm\frac{5}{2}\leftrightarrow\pm\frac{7}{2}$ and $\pm\frac{3}{2}\leftrightarrow\pm\frac{5}{2}$ (Table VI). This rather good agreement confirms that the relaxation is caused by magnetic fluctuations and that the spectral density of fluctuating fields is nearly independent on the frequency.

For the Co1a and Co1b sites, it was found that T_1 values for the $\pm\frac{5}{2}\leftrightarrow\pm\frac{7}{2}$ are shorter than that for $\pm\frac{3}{2}\leftrightarrow\pm\frac{5}{2}$ (Table VI). This effect does result in that case from the proximity of the fast relaxing Co2 $\pm\frac{3}{2}\leftrightarrow\pm\frac{5}{2}$ transitions (see Fig. 4) which induce by cross-relaxation processes a reduction of the recovery time on the $\pm\frac{5}{2}\leftrightarrow\pm\frac{7}{2}$ transitions of Co1a and Co1b. For these Co1 sites, the T_1 value retained then hereafter is the longer one deduced from the $\pm\frac{3}{2}\leftrightarrow\pm\frac{5}{2}$ transition data.

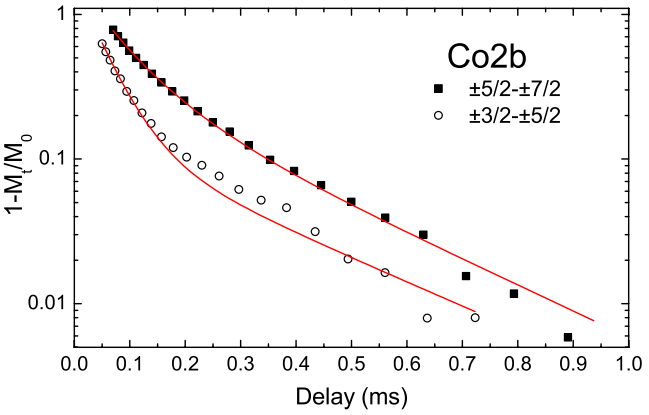

FIG. 7. (Color online) Spin-lattice relaxation curves for Co2b site measured at 7.52 and 4.83 MHz ($\pm\frac{5}{2}\leftrightarrow\pm\frac{7}{2}$ and $\pm\frac{3}{2}\leftrightarrow\pm\frac{5}{2}$ transitions respectively) at 4.2 K. Solid lines are the fits of experimental points by the magnetization relaxation functions (4) with parameters from the Table V.

In Fig. 8, we show the temperature dependence of nuclear spin-lattice relaxation rates $1/T_1$ for all four cobalt sites. As one can see for both Co2a and Co2b, NSLR is about 2 orders of magnitude larger than for Co1a and Co1b. As was already stated in Ref. 9, this proves the nonmagnetic nature of Co1 sites. Also Fig. 8, shows that $1/T_1$ increases with T at low temperatures. Above 20 K, the NSLR becomes so fast that we loose then the Co2 NQR signals. Measurements at higher T cannot be carried out then by NQR and T_1 evolution will be rather studied by NMR as will be discussed in a forthcoming paper.[20] Similarly, the spin-lattice relaxation measurements for ^{23}Na were technically challenging and have therefore not been performed here as they have been studied in great detail by NMR in Ref. 10 for various Na_xCoO_2 phases including the $x=2/3$ phase.

B. Spin-spin relaxation and signal intensities

NSSR is a complex phenomenon, but at its most fundamental level, the random fluctuations of the local magnetic field lead to a loss of the initial phase coherence of the nuclear spins and therefore to the decrease of the transverse nuclear-spin magnetization. In the Redfield theory,[21] the transverse relaxation arises from two mechanisms: (1) nuclear spin-spin coupling (via magnetic dipolar or indirect interactions) and (2) the spin-lattice relaxation.

The NSSR is studied by monitoring the spin-echo intensity as a function of the time delay τ between $\pi/2$ and π pulses. In general, the decay of transverse magnetization $M(t)$ as a function of time $t=2\tau$ can be fitted by the equation

$$M(t)=M(0)\exp\left[-\left(\frac{t}{T_2}\right)^n\right]. \tag{5}$$

The NSSR process is characterized by the relaxation time T_2 and the exponent n, which characterizes the decay shape which usually varies between Lorentzian ($n=1$) and Gaussian ($n=2$).

TABLE VI. ^{59}Co relaxation and NQR linewidth parameters (see text for details).

Site	Co1a	Co1b	Co1a	Co1b	Co2b	Co2a	Co2b
Transition	$\pm\frac{3}{2}\leftrightarrow\pm\frac{5}{2}$	$\pm\frac{3}{2}\leftrightarrow\pm\frac{5}{2}$	$\pm\frac{5}{2}\leftrightarrow\pm\frac{7}{2}$	$\pm\frac{5}{2}\leftrightarrow\pm\frac{7}{2}$	$\pm\frac{3}{2}\leftrightarrow\pm\frac{5}{2}$	$\pm\frac{5}{2}\leftrightarrow\pm\frac{7}{2}$	$\pm\frac{5}{2}\leftrightarrow\pm\frac{7}{2}$
ν (MHz)	2.387(1)	2.785(1)	3.581(2)	4.178(1)	4.826(2)	6.473(1)	7.524(1)
T_1 (ms)	40.5(5)	55.5(5)	26(1)	46(2)	0.8(1)	0.59(3)	0.73(4)
T_2 (μs)	316(4)	326(7)	320(2)	335(6)	30(2)	71(2)	49(2)
n	2	2	2	2	1	1	1
T_1' (ms)	2.3	3.2	2.6	4.6	0.050	0.058	0.072
α					0.61(5)	1.20(8)	0.67(5)
$\Delta\nu_{calc}$ (kHz)	1.0(4)	0.9(2)	1.0(2)	0.9(2)	10.6(3)	4.5(3)	6.5(2)
$\Delta\nu$ (kHz)	12.8(9)	12.1(8)	18.6(9)	18.3(8)	42(2)	24(1)	24(1)

1. ^{23}Na spin-spin relaxation

The spin-spin relaxation decays for sodium sites are shown in Fig. 9. The shortest τ value used was only ≈ 65 μs due to the long dead time τ_D of the spectrometer (see Sec. III). Then the beginnings of the relaxation decays were lost and only tails were measured. Therefore, it was impossible to determine reliably the transverse magnetization decay shape. Nevertheless, the experimental data were fitted by a Lorentzian ($n=1$) function [see Eq. (5)] in order to obtain estimates of the spin-spin relaxation times and of the NQR lines intensities. The T_1 values of ^{23}Na known from the data of Ref. 10 for the same phase of sodium cobaltates were long enough to ascertain that they do not contribute significantly to the transverse magnetization decay. So the values obtained by fitting the relaxation decays for the sodium sites given in Table VII can be associated with spin-spin processes.

The values of magnetization at zero time $M(0)$ after ν^2 frequency correction allowed us to estimate the relative intensities of sodium lines (sites) which are also reported in Table VII. These data are in good agreement with the more accurate ones obtained by NMR. Here, the accuracy[9] is indeed limited primarily by the extrapolation required from τ_D to $\tau=0$ and also by the variation of spectrometer sensitivity with frequency.

Due to the NSSR process, the linewidth of an NQR signal at half-height should be equal $\Delta\nu_{calc}=1/(\pi T_2)$.[16] Such $\Delta\nu_{calc}$ for different Na sites are also collected in Table VII. And it is easy to see that they are approximately 3 times smaller than the experimentally measured linewidths for all sodium sites (Table VII). This clearly shows that the experimentally observable Na lines are inhomogeneously broadened by a weak distribution of EFG such that $\Delta\nu_Q/\nu_Q\approx 4\times 10^{-3}$. Such a small value found indeed implies a very well-ordered structure in the sodium layers of this $Na_{2/3}CoO_2$ compound.

2. ^{59}Co spin-spin relaxation

The transverse relaxation decays for ^{59}Co sites are represented in Fig. 10, where panel (a) shows data for the $\pm\frac{3}{2}\leftrightarrow\pm\frac{5}{2}$ transitions of the Co1a and Co1b sites and panel (b) that for the $\pm 7/2\leftrightarrow\pm 5/2$ transitions of the Co2a and Co2b sites. The results of the fit of these curves by Eq. (5) are summarized in the Table VI. For the Co1 sites, the transverse magnetization decay has a Gaussian form ($n=2$); for Co2 it is a Lorentzian with $n=1$. To understand this difference, one needs to analyze the possible influence of spin-lattice relaxation on the transverse relaxation.

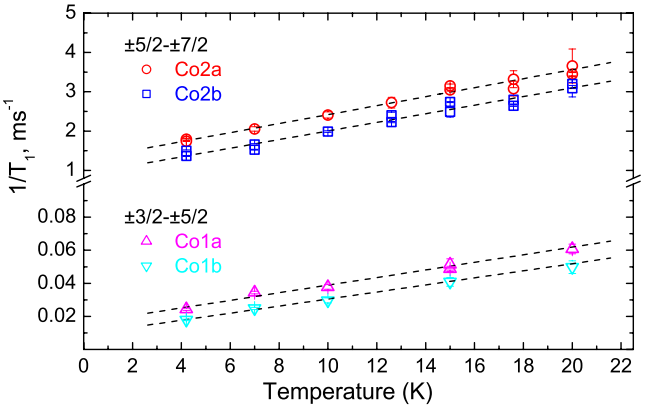

FIG. 8. (Color online) Temperature dependence of nuclear spin-lattice relaxation rates $1/T_1$ for all four cobalt sites in the $Na_{2/3}CoO_2$ compound. For Co1a and Co1b, measurements were done on the $\pm\frac{3}{2}\leftrightarrow\pm\frac{5}{2}$ transitions and for Co2a and Co2b, measurements were done on the $\pm\frac{5}{2}\leftrightarrow\pm\frac{7}{2}$ transitions. Linear fits shown by dotted lines are guides to the eyes.

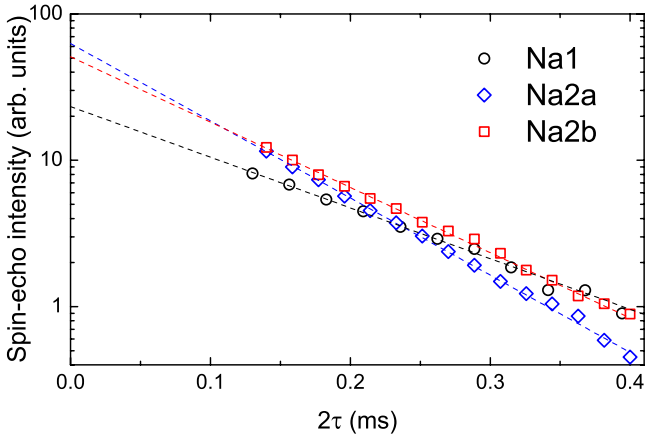

FIG. 9. (Color online) Spin-spin relaxation curves of ^{23}Na sites and fits by the Eq. (5).

TABLE VII. ^{23}Na relaxation and NQR linewidth parameters.

Site	I (%)	T_2 (μs)	$\Delta\nu_{calc}$ (kHz)	$\Delta\nu$ (kHz)
Na1	23(5)	125(2)	2.5(1)	8.2(1)
Na2a	46(8)	82.3(7)	3.8(2)	8.21(5)
Na2b	31(7)	97(1)	3.3(2)	9.02(6)

For the cobalts, the spin-lattice relaxation is fast enough so its contribution to the spin-spin relaxation becomes important. As the spin-lattice relaxation of ^{59}Co is multiexponential [Eq. (4)], then a good approximation might be done by considering that T_2 in the Eq. (5) should be related to the slope of the NSLR curves T_1' at short times. For example, the Eq. (4) with the parameters from the Table V can be written, at short-enough times for the Co2b's $\pm\frac{5}{2}\leftrightarrow\pm\frac{7}{2}$ transition as

$$R(t) \approx 1 - \frac{10.12t}{T_1} = 1 - \frac{t}{T_1'}.$$

In Table VI, one can see the estimated values of T_1' for different Co sites and transitions. For Co1a and Co1b, these T_1' times are much longer than the spin-spin relaxation T_2 in Fig. 10(a). Therefore, the NSLR contribution to the NSSR is negligible and we see in experiments the real spin-spin relaxation of Co1 sites. But for Co2, the calculated T_1' values become comparable to the obtained T_2 times. To emphasize this, we reported in the Table VI the ratio $\alpha=T_2/T_1'$. As one can see, α is almost the same for the two measured transitions $\pm\frac{5}{2}\leftrightarrow\pm\frac{3}{2}$ and $\pm\frac{7}{2}\leftrightarrow\pm\frac{5}{2}$ for the Co2b site. So we conclude that for Co2 sites, the measured T_2 values are determined by spin-lattice relaxation process. This explains as well the difference in the transverse magnetization decay shape for Co1 and Co2 sites.

This influence of spin-lattice relaxation on the spin-spin relaxation explains why the intensity of the low-frequency transitions of Co2a and Co2b sites are found so weak experimentally (see Fig. 4). As one can see from the Table VI, for the Co2b site, the measured $T_2=30(2)$ μs for the $\pm\frac{3}{2}\leftrightarrow\pm\frac{5}{2}$ transition is smaller than that [49(2) μs] for the $\pm\frac{5}{2}\leftrightarrow\pm\frac{7}{2}$ transition. Also as was already stated in Sec. III, the minimum usable time τ_D between rf pulses increases with decreasing frequency. So, both factors reduce the intensities of the observed low-frequency Co2 NQR lines.

As has been noticed previously in Sec. III, the signal intensities observed at different frequencies are affected by the variation of spectrometer sensitivity, so careful determination of the relative site occupancies of Co1 and Co2 could not be done directly from our experiments. But we could estimate the fractional occupancies inside each group of cobalt (Co1 and Co2) separately, as their resonance frequencies are close. After correcting for the spin-spin relaxation T_2 and for the ν^2 frequency dependence of the signal intensity, we obtained Co1a/Co1b=1.95(0.1) and Co2b/Co2a=1.9(0.2), in agreement with similar determinations from ^{59}Co NMR, which allowed as well better determinations of the Co1:Co2 ratio.[10]

Spectral lines of cobalt are inhomogeneously broadened (see Table VI) and this is clear if one compares the experimental linewidth to the calculated one. Notice that the ratio $\Delta\nu/\Delta\nu_{calc}$ is $\approx$4.0(0.4) for both $\pm\frac{3}{2}\leftrightarrow\pm\frac{5}{2}$ and $\pm\frac{5}{2}\leftrightarrow\pm\frac{7}{2}$ transitions of Co2b and $\approx$5.0(0.3) for Co2a, which confirms that these broadenings have the same origin.

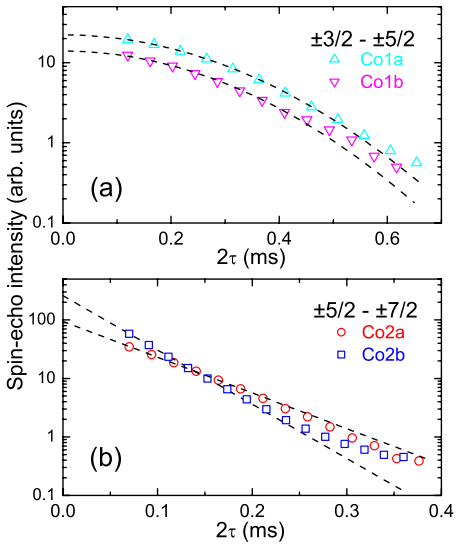

FIG. 10. (Color online) (a) Spin-spin relaxation curves for Co1a and Co1b sites on $\pm3/2\leftrightarrow\pm5/2$ transition and (b) for Co2a and Co2b on $\pm5/2\leftrightarrow\pm7/2$ transition.

V. CONCLUSION

In summary, we have reported detailed powder x-ray and NQR data for the $Na_{2/3}CoO_2$ compound supporting the recent paper[9] in which we proposed a detailed structural model for this material from NMR and NQR results. The NQR spectrum of ^{23}Na and ^{59}Co consists of several narrow lines, which could be associated with three sodium and four cobalt sites, in a 2D unit cell comprising eight Na sites over 12 Co. The finite number of inequivalent site positions confirms that the simple 3D ordering of the Na layers leads to a differentiation of cobalt sites. We have performed as well a careful Rietveld analysis of the x-ray data which confirms the atomic 3D unit cell proposed from NMR and NQR. The best Rietveld fits allowed us to determine the slight atomic displacements of the Na atoms in the model unit cell. Also, the quality of the fit allows us to ascertain the $x=2/3$ value of the Na content.

Others have also detected this phase and identified it with the present one from its large spin susceptibility at low temperatures.[11] They have performed single-crystal diffraction experiments in which they also find a 12-Co 2D unit cell. Using chemical analyses of their single crystals, they proposed that $x=0.71$ and have elaborated then a structural model in which the concentration of Na alternates between planes with $x=2/3$ with eight Na per 2D cell and $x=3/4$, with nine Na per 2D cell. In these Na layers, the Na vacancies would be alternatively organized in divacancies and trivacancies. One can immediately see that such a structure would never explain the present NMR and NQR data as it corresponds to a larger number of distinct Na sites (three in

each Na plane) than found experimentally. Furthermore, the only sites exhibiting the threefold symmetry and $\eta=0$ would then be the Na1 sites of the $x=2/3$ planes. The fraction of such sites would be $x=2/17$, nearly twice smaller than the $25\%=2/8$ found experimentally.

The spin-spin and spin-lattice relaxations of the NQR lines were studied for all Co sites and the data analysis has allowed us to demonstrate that both T_1 and T_2 data do allow to establish the difference of magnetic properties of the two types of Co sites. As indicated in Ref. 9, they constitute two sublattices: a kagome structure for the magnetic sites and the complementary triangular lattice of nonmagnetic Co sites involving 25% of the Co.

Beyond the simple results obtained for this $Na_{2/3}CoO_2$ compound, the approach developed here will be certainly useful to perform structural determinations for pure phases with different Na contents for which an ordering has been evidenced. We have indeed isolated some of them both below[3] and above $x=0.65$,[10] which display quite distinct ground-state physical properties. This might apply as well for the phases detected for larger x values.[23,24]

ACKNOWLEDGMENTS

We thank N. Blanchard for her help in synthesizing materials and Y. S. Meng for numerous exchanges about their computations. We acknowledge financial support by the ANR (Grant No. NT05-441913) in France and by the Grant No. RNP-6183 in Russia. Expenses in Orsay for I.R.M. and A.V.D. have been supported by the "Triangle de la Physique."

*irek.mukhamedshin@ksu.ru

[1] I. Terasaki, Y. Sasago, and K. Uchinokura, Phys. Rev. B **56**, R12685 (1997).
[2] K. Takada, H. Sakurai, E. Takayama-Muromachi, F. Izumi, R. A. Dilanian, and S. Sasaki, Nature (London) **422**, 53 (2003).
[3] G. Lang, J. Bobroff, H. Alloul, G. Collin, and N. Blanchard, Phys. Rev. B **78**, 155116 (2008).
[4] G. Lang, J. Bobroff, H. Alloul, P. Mendels, N. Blanchard, and G. Collin, Phys. Rev. B **72**, 094404 (2005).
[5] C. de Vaulx, M.-H. Julien, C. Berthier, M. Horvatić, P. Bordet, V. Simonet, D. P. Chen, and C. T. Lin, Phys. Rev. Lett. **95**, 186405 (2005).
[6] H. W. Zandbergen, M. L. Foo, Q. Xu, V. Kumar, and R. J. Cava, Phys. Rev. B **70**, 024101 (2004).
[7] P. H. Zhang, R. B. Capaz, M. L. Cohen, and S. G. Louie, Phys. Rev B **71**, 153102 (2005).
[8] J. Bobroff, G. Lang, H. Alloul, N. Blanchard, and G. Collin, Phys. Rev. Lett. **96**, 107201 (2006).
[9] H. Alloul, I. R. Mukhamedshin, T. A. Platova, and A. V. Dooglav, EPL **85**, 47006 (2009).
[10] H. Alloul, I. R. Mukhamedshin, G. Collin, and N. Blanchard, EPL **82**, 17002 (2008).
[11] F. C. Chou, M.-W. Chu, G. J. Shu, F.-T. Huang, W. W. Pai, H. S. Sheu, and P. A. Lee, Phys. Rev. Lett. **101**, 127404 (2008).
[12] Y. Hinuma, Y. S. Meng, and G. Ceder, Phys. Rev. B **77**, 224111 (2008).
[13] J. D. Jorgensen, M. Avdeev, D. G. Hinks, J. C. Burley, and S. Short, Phys. Rev. B **68**, 214517 (2003).
[14] Q. Huang, M. L. Foo, R. A. Pascal, Jr., J. W. Lynn, B. H. Toby, T. He, H. W. Zandbergen, and R. J. Cava, Phys. Rev. B **70**, 184110 (2004).
[15] I. R. Mukhamedshin, H. Alloul, G. Collin, and N. Blanchard, Phys. Rev. Lett. **93**, 167601 (2004).
[16] A. Abragam, *The Principles of Nuclear Magnetism* (Clarendon Press, London, 1961).
[17] W. G. Clark, M. E. Hanson, F. Lefloch, and P. Segransan, Rev. Sci. Instrum. **66**, 2453 (1995).
[18] A. P. Bussandri and M. J. Zuriaga, J. Magn. Reson. **131**, 224 (1998).
[19] I. R. Mukhamedshin, H. Alloul, G. Collin, and N. Blanchard, Phys. Rev. Lett. **94**, 247602 (2005).
[20] I. R. Mukhamedshin and H. Alloul (unpublished).
[21] C. P. Slichter, *Principles of Magnetic Resonance*, 2nd ed. (Springer, New York, 1980).
[22] J. Chepin and J. H. Ross, J. Phys.: Condens. Matter **3**, 8103 (1991).
[23] M. Roger, D. J. P. Morris, D. A. Tennant, M. J. Gutmann, J. P. Goff, J.-U. Hoffmann, R. Feyerherm, E. Dudzik, D. Prabhakaran, A. T. Boothroyd, N. Shannon, B. Lake, and P. P. Deen, Nature (London) **445**, 631 (2007).
[24] T. F. Schulze, P. S. Hafliger, Ch. Niedermayer, K. Mattenberger, S. Bubenhofer, and B. Batlogg, Phys. Rev. Lett. **100**, 026407 (2008).